Sensors and Materials, Vol. 37, No. 4 (2025) 1333–1349
MYU Tokyo

S & M 3990

Quantitative Assessment of Chl *a* and *b* in Spinach Chl Standard Solution Using a Filter-free Wavelength Sensor

Ryoma Mibu, Yong-Joon Choi,* Tomoya Ide, Yasuyuki Kimura, Kazuhiro Takahashi, Toshihiko Noda, Kotaro Takayama, and Kazuaki Sawada

Department of Electrical and Electronic Information Engineering, Toyohashi University of Technology, Hibarigaoka1-1 Tempakucho, Toyohashi, Aichi 441-8580, Japan

(Received November 7, 2024; accepted March 12, 2025)

Keywords: filter-free wavelength sensor, optical sensor, chlorophyll a, b, photosynthetic pigment, agriculture

We proposed a quantitative method for assessing chlorophyll (Chl) content and Chl *a*/*b* ratio using a filter-free wavelength sensor. Initially, an experiment was conducted to simulate changes in Chl *a* and *b* by adjusting the light intensity at wavelengths of 650 and 660 nm. The sensor's output current ratio exhibited a linear relationship with the light intensity, suggesting its potential for measuring Chl. Subsequently, measurements were performed using standard Chl *a* and *b* solutions. A strong linear correlation was observed between sensor output and Chl content, independent of changes in Chl *a*/*b* ratio. However, no direct correlation was found between sensor output and Chl *a*/*b* ratio. This inconsistency was attributed to the varying impact of Chl content changes on the sensor output, depending on the specific Chl *a*/*b* ratio. To address this limitation, we proposed a calibration method based on the relationship between Chl content and sensor output. By applying this calibration curve, we successfully reduced the error in Chl *a*/*b* ratio measurements. This approach enables the use of filter-free wavelength sensors for the accurate quantification of Chl content and Chl *a*/*b* ratio, offering a potential solution for on-site monitoring and agricultural applications.

1. Introduction

In recent years, the global population has been steadily increasing. The United Nations announced in July 2024 that the world's population would continue to grow for the next 60 years, reaching 10.3 billion in 2080.[1] This trend has raised concerns about food security, especially in countries like Japan facing an aging population and a declining number of farmers.[2–4] Ensuring a stable food supply necessitates attracting new farmers to agriculture. However, agriculture involves numerous complex techniques that can be difficult to learn and master, particularly owing to the annual cycle of crop growth.[5] To address these challenges, smart agriculture, incorporating robotics and information and communication technology, has gained popularity.[6–8] Optimizing growth conditions in controlled plant cultivation environments is

*Corresponding author: e-mail: choi@ee.tut.ac.jp
https://doi.org/10.18494/SAM5455

ISSN 0914-4935
https://myukk.org/

crucial for increasing productivity. This requires the accurate measurement of plant biological information, including photosynthesis, which is essential for plant growth as it converts light energy into chemical energy.[9,10]

Photosynthesis is carried out by chlorophyll (Chl), a pigment found in plants. Land plants contain Chl *a* and *b*.[11–13] Chl *a* is the photosynthetic component, whereas Chl *b* serves as an auxiliary component, acting as an antenna to capture light.[14,15] The total amount of Chl *a* and *b*, known as Chl content, is a valuable indicator of plant growth conditions. Chl meters are widely used in agriculture and research owing to their simplicity in measuring Chl content.[16–18] Furthermore, the ratio of Chl *a* to Chl *b* (Chl *a*/*b* ratio) can be used to assess the light environment in plants. This ratio varies depending on light conditions. Under high-light conditions, plants tend to replace Chl *b* with Chl *a* to enhance photosynthetic efficiency, increasing the Chl *a*/*b* ratio. Conversely, plants may convert Chl *a* to Chl *b* under lowlight conditions to capture more light, leading to a decrease in Chl *a*/*b* ratio.[19,20] Traditional methods for measuring the Chl *a*/*b* ratio, such as spectrophotometry and high-performance liquid chromatography, often involve large-scale equipment, expensive instruments, and specialized expertise, making them impractical for widespread agricultural applications.[21–23]

To address these challenges, our research group fabricated a filter-free wavelength sensor that can detect wavelength information without optical components. Using this sensor, we previously reported a compact Chl detection system suitable for agricultural applications.[24–26] Although we could estimate changes in Chl *a*/*b* ratio according to spectral changes in tomato leaves, quantitative analysis was limited. In this paper, we report a thorough investigation into the factors affecting Chl *a*/*b* ratio measurements using our filter-free wavelength sensor and propose a quantitative assessment method for Chl content and Chl *a*/*b* ratio.

2. Principle

2.1 Filter-free wavelength sensor

Figure 1 shows a cross section and potential distribution diagram of the filter-free wavelength sensor. The sensor features a double-diffusion well structure with deep *n*- and *p*-wells on a *p*-substrate. By applying voltage to the photogate (PG), a potential peak *W* is formed in the sensor. When light is incident on the sensor, the generated photoelectrons are divided between the surface and substrate sides of the sensor at the potential peak *W*. The surface current I_{FD} and the substrate current I_{NW} are read from the respective electrodes of the sensor. Equations (1) and (2) describe I_{FD} and I_{NW}, respectively, while the sum of these currents ($I_{FD} + I_{NW}$) can be used to calculate the incident light intensity according to Eq. (3).

$$I_{FD} = -\frac{qS\lambda}{hc}\left(1 - e^{-\alpha W}\right)\phi_0 \tag{1}$$

$$I_{NW} = -\frac{qS\lambda}{hc}\left(e^{-\alpha W} - e^{-\alpha W_{np}}\right)\phi_0 \tag{2}$$

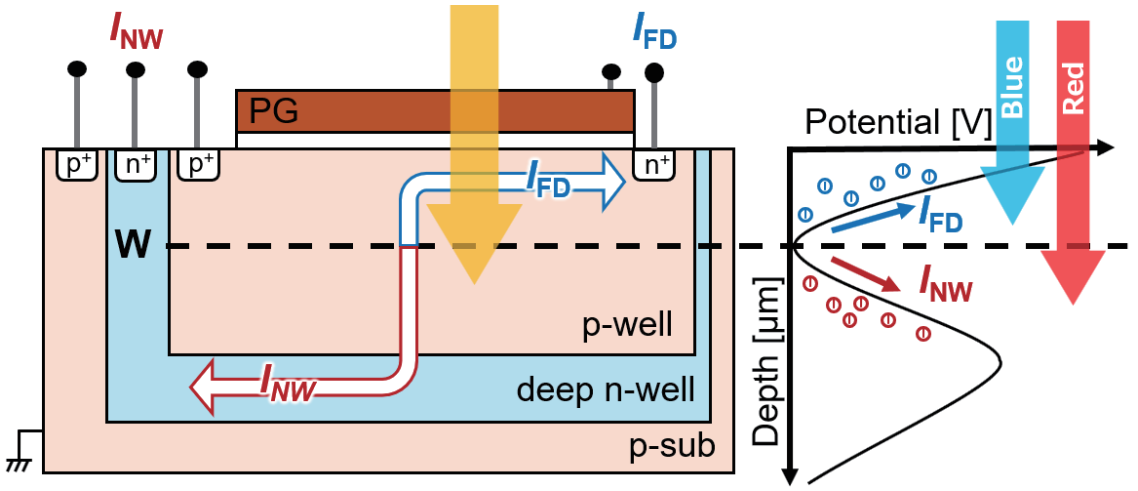

Fig. 1. (Color online) Cross section and electrons in the filter-free wavelength sensor at different incident wavelengths.

$$I_{total} = I_{FD} + I_{NW} = -\frac{qS\lambda}{hc}\left(1 - e^{-\alpha W_{np}}\right)\phi_0 \tag{3}$$

Here, q is the charge, S is the photosensitive area, λ is the wavelength, h is Planck's constant, c is the speed of light, α is the absorption coefficient of silicon, W is the potential peak depth, W_{np} is the junction depth between p- and n-wells, and ϕ_0 is the incident light intensity.

By using the difference in the penetration depth of light into silicon at various wavelengths, it is possible to determine the wavelength from the ratio of the two currents.[27–29] For instance, when the sensor is irradiated with blue light, which has a short wavelength, I_{NW} is low and I_{FD} is high owing to the light being absorbed near the surface of the sensor. Consequently, the sensor current ratio (I_{NW}/I_{FD}) is low. In contrast, red light with a longer wavelength is absorbed deeper within the sensor, leading to a higher I_{NW} current and a lower I_{FD} current, resulting in a higher sensor current ratio. Therefore, the wavelength can be distinguished from the current ratio of the sensor. Notably, the sensor current ratio shown in Eq. (4) solely depends on the potential peak W and the absorption coefficient of silicon, independent of light intensity.

$$\frac{I_{NW}}{I_{FD}} = \frac{e^{-\alpha W} - e^{-\alpha W_{np}}}{1 - e^{-\alpha W}} \tag{4}$$

For broad light sources with multiple spectral peaks, the centroid wavelength λ_c can be calculated and correlated with the sensor characteristics. The centroid wavelength λ_c represents the weighted average wavelength of the spectrum and can be determined using Eq. (5).

$$\lambda_c = \frac{\int \lambda\phi(\lambda)d\lambda}{\int \phi(\lambda)d\lambda} \tag{5}$$

2.2 Chl quantitative method using filter-free wavelength sensor

2.2.1 Chl content

The transmittance measurement is performed using the system shown in Fig. 2(a). A 660 nm light source uses a standardized quartz cuvette (which has a fixed optical path length) to measure Chl solutions extracted from leaves using an organic solvent or standard solution. For transmittance measurement, a 660 nm LED light source (M660FP1, Thorlabs) is used, which corresponds to the absorption peaks of Chl *a* and *b*. In this wavelength range, it is not affected by interference from other photosynthetic pigment components. Additionally, the light source's full width at half maximum (FWHM) must cover both Chl *a* and *b* absorption peaks. (In this experiment, the FWHM is 25 nm.)

The relative content of Chl can be estimated by comparing the current generated by the transmitted light in a reference solution without Chl (I_{Ref}) and that in the Chl solution (I_{Chl}). Figure 2(b) shows the change in the intensity of transmitted light when illuminated with 660 nm light. In transmittance measurements, the light intensity is calculated from the sum of the surface and substrate currents. In the reference solution without Chl, a spectrum with a peak at 660 nm, as shown by the black line, is obtained. On the other hand, in the Chl solution, the transmitted light spectrum changes, as indicated by the green line, owing to light absorption by Chl *a* and *b*. The transmittance is then calculated using Eq. 6, and the measurement can be performed by correlating it with the Chl content.

$$Chl\ content\left(Transmittance\right) = -\log_{10}\left(\frac{I_{Chl}}{I_{Ref}}\right) = -\log_{10}\frac{I_{\mathrm{FD}} + I_{\mathrm{NW}}\left(\text{Chl solution}\right)}{I_{\mathrm{FD}} + I_{\mathrm{NW}}\left(\text{Reference solution}\right)} \tag{6}$$

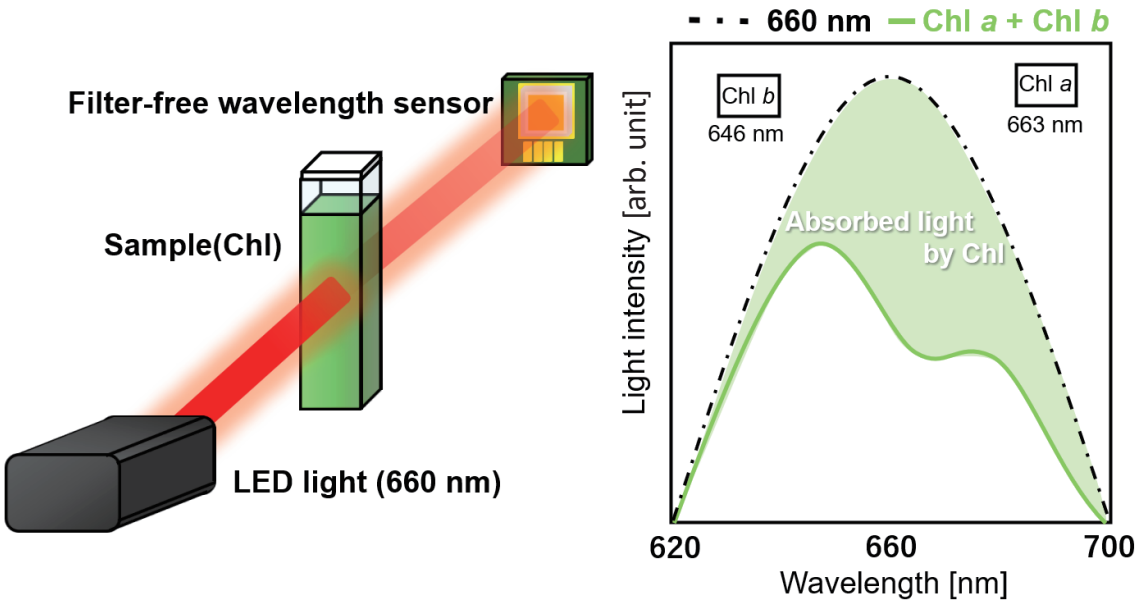

(a) (b)

Fig. 2. (Color online) (a) Measurement setup for Chl measurement and (b) transmitted light intensity changes by Chl content.

2.2.2 Chl *a*/*b* ratio

Chl *a* and *b* absorb light primarily at wavelengths near 663 and 646 nm, respectively.[24,26] By irradiating leaves with a 660 nm LED light source, which encompasses the absorption wavelengths of both Chl *a* and *b*, the transmitted light spectrum varies depending on the relative abundance of these pigments.

Figure 3 illustrates the transmitted light spectral changes when a leaf is irradiated with 660 nm light. In Fig. 3(a), where the Chl *a*/*b* ratio is low, Chl *b* absorbs more light at wavelengths shorter than 660 nm, causing a red-shift in centroid wavelength. Conversely, in Fig. 3(b), where the Chl *a*/*b* ratio is high, Chl *b* absorbs more light at wavelengths longer than 660 nm, resulting in a blue-shift in centroid wavelength. Therefore, by measuring the shift in centroid wavelength, this sensor can be used to determine the Chl *a*/*b* ratio.[26]

2.3 Chl measurement by spectrometer

Chl *a* and *b* exhibit strong absorption properties in the blue wavelength range ($\lambda \approx 450$ nm) and red wavelength range ($\lambda \approx 650$ nm), respectively. However, in the blue wavelength range, carotenoids also absorb light, making it challenging to selectively quantify the Chl component.[30] Consequently, Chl absorbance measurements are typically conducted in the red wavelength range, and various quantitative equations have been proposed for determining Chl content. While Arnon's equation remains in use, it is generally not recommended.[31,32] Among the

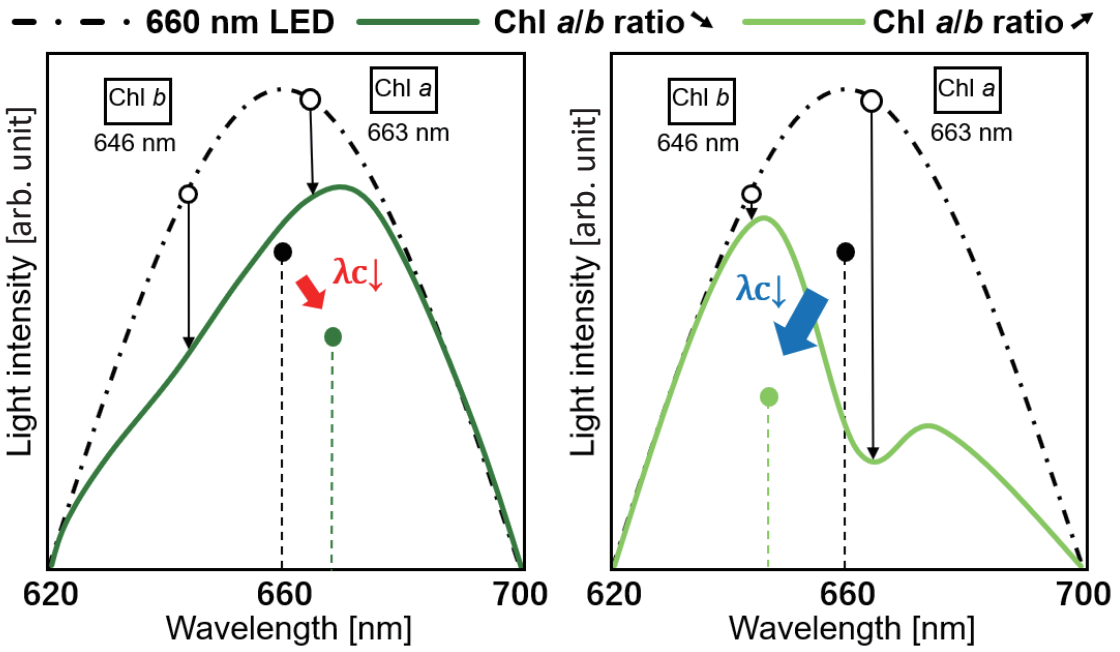

Fig. 3. (Color online) Changes in transmitted light intensity when the Chl *a*/*b* ratio is (a) low and (b) high. The centroid wavelength λ_c changes according to spectral changes.

available equations, Porra's equations, which utilize N, N-dimethylformamide (DMF) for extraction, are currently considered the most accurate.[33] Equations (6) to (8) are Porra's equations for determining Chl content from absorbance measurements.[34]

$$Chl\,a\left[\mu\mathrm{M}\right] = 13.43A^{663.8\,\mathrm{nm}} - 3.47A^{646.8\,\mathrm{nm}} \tag{6}$$

$$Chl\,b\left[\mu\mathrm{M}\right] = 22.90A^{646.8\,\mathrm{nm}} - 5.38A^{663.8\,\mathrm{nm}} \tag{7}$$

$$Chla\,a+b\left[\mu\mathrm{M}\right] = 19.43A^{646.8\,\mathrm{nm}} + 8.05A^{663.8\,\mathrm{nm}} \tag{8}$$

Here, A^{λ} represents the absorbance peak at wavelength λ. The absorbance values at 663.8 and 646.8 nm, corresponding to the absorption peaks of Chl *a* and *b*, respectively, are used in the calculations.

3. Experimental Results

3.1 Characteristics of light sources

3.1.1 Measurement configuration

Figure 4 shows the measurement system. Two xenon light sources (MAX-350, Asahi Spectra) were used: one equipped with an interference band pass filter centered at 660 nm (HMX0660, Asahi spectra) with a FWHM of 14.7 nm to simulate Chl *a* absorption, and the other with a filter centered at 650 nm (HMX0650, Asahi spectra) and an FWHM of 12.7 nm to simulate Chl *b* absorption. Light from the sources was irradiated to a spectrometer (USB4000, Ocean Insight) or a filter-free wavelength sensor via a split optical fiber (SPLIT400-UV-VIS, Ocean Insight). In this experiment, the Chl *a*/*b* ratio was simulated by adjusting the light intensity under the conditions outlined in Table 1.

3.1.2 Experimental results

Figure 5(a) shows the spectra obtained from the spectrometer, showing that the spectra change with the Chl *a*/*b* ratio. The centroid wavelength shifts toward shorter wavelengths as the Chl *a*/*b* ratio increases. Figure 5(b) shows the centroid wavelength calculated from the spectrum and the sensor current ratio. It can be seen that there is a high linearity in the sensor current ratio as the centroid wavelength changes. Since the plot variation occurs in both the spectrometer data and the sensor data, we consider that it is caused by the fluctuation of the light source. The sensor current during measurement is approximately 250 pA for the surface current and approximately 500 pA for the substrate current. The sensor fluctuation is a maximum of 7 pA for the surface current and a maximum of 0.6 pA for the substrate current. The signal-to-noise (S/N)

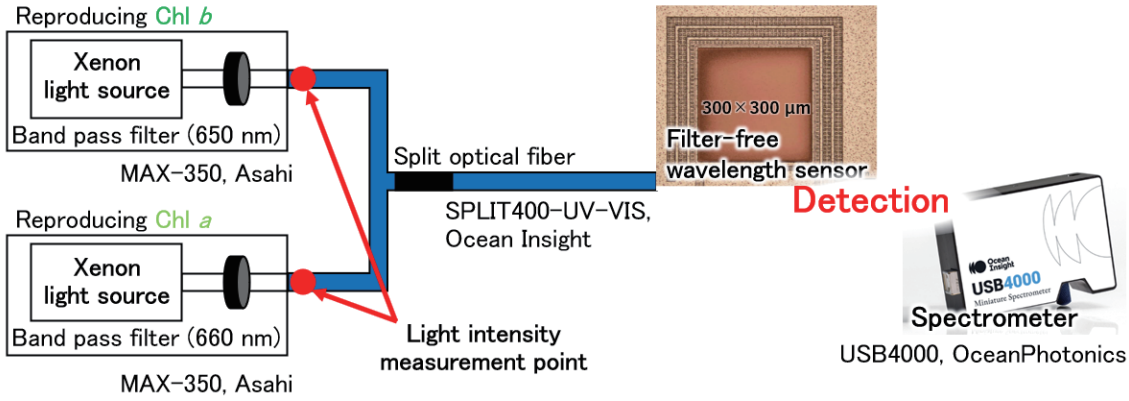

Fig. 4. (Color online) Experimental setup for reproducible measurements. Band pass filters were mounted on each xenon light source. A split optical fiber was used to illuminate the spectrometer and sensor simultaneously.

Table 1
Light intensity conditions for reproducing Chl *a*/*b* ratios.

Chl *a* (660 nm light)	Chl *b* (650 nm light)	Chl *a*/*b* ratio (Light intensity ratio)
2.0 (ϕ : 72.8 mW/cm^2)	0.5 (ϕ : 29.7 mW/cm^2)	4.0 (3.9)
	1.0 (ϕ : 17.8 mW/cm^2)	2.0 (1.9)
	1.5 (ϕ : 8.5 mW/cm^2)	1.3 (1.1)
3.0 (ϕ : 53.5 mW/cm^2)	0.5 (ϕ : 29.7 mW/cm^2)	6.0 (6.3)
	1.0 (ϕ : 17.8 mW/cm^2)	3.0 (3.0)
	1.5 (ϕ : 8.5 mW/cm^2)	2.0 (1.8)
4.0 (ϕ : 33.2 mW/cm^2)	0.5 (ϕ : 29.7 mW/cm^2)	8.0 (8.5)
	1.0 (ϕ : 17.8 mW/cm^2)	4.0 (4.1)
	1.5 (ϕ : 8.5 mW/cm^2)	2.7 (2.5)

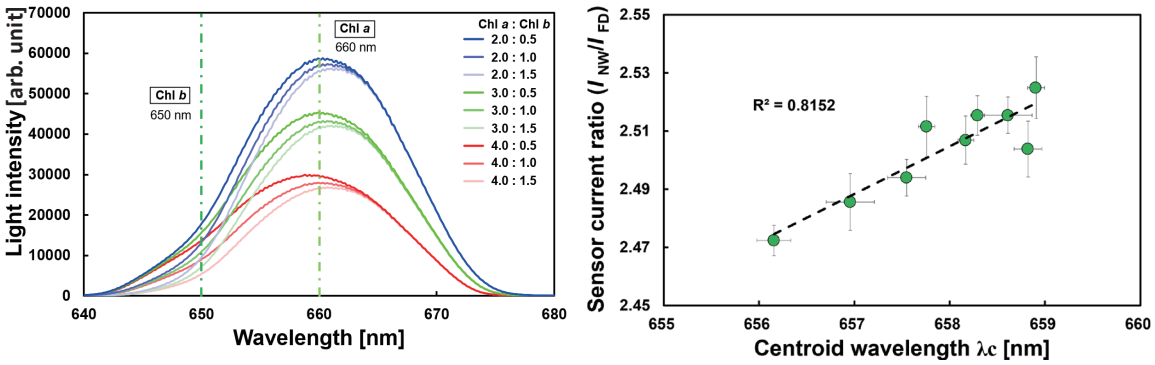

(a) (b)

Fig. 5. (Color online) (a) Transmitted light spectrum and (b) relationship between the centroid wavelength λ_c and filter-free wavelength sensor current ratio. As the Chl *b* concentration increases (Chl *a*/*b* ratio decreases), the centroid wavelength λ_c shifts toward shorter wavelengths.

ratio corresponds to approximately 31.1 dB for the surface current and approximately 58.4 dB for the substrate current. Therefore, it was shown that it is possible to measure the Chl *a*/*b* ratio change by measuring the sensor current ratio.

3.2 Measurement of Chl *a* and *b* standard solutions

3.2.1 Measurement configuration

Figure 6 shows the measurement system used for Chl assessment. An LED light source (M660FP1, Thorlabs) with a 25 nm FWHM and a 660 nm wavelength was utilized. This wavelength range encompasses the absorption peaks of both Chl *a* and *b*. The light intensity was adjusted to 121.6 mW/cm², ensuring that sufficient transmitted light was obtained without being affected by the sensor's dark current. The transmitted light from the sample was simultaneously detected by a spectrometer (USB4000, Ocean Insight) and a filter-free wavelength sensor. These two detection methods, commonly used in modern Chl measurements, were compared using a split optical fiber (SPLIT400-UV-VIS, Ocean Insight).

Figure 7 shows the prepared Chl samples. A total of 55 samples were created by mixing two types of standard solution, namely, Chl *a* standard solution (96145-1MG, Supelco) and Chl *b* standard solution (00538-1MG, Supelco). The Chl content of these samples ranged from 2 to 18 μM, whereas the Chl *a*/*b* ratio varied from 2.0 to 4.0.

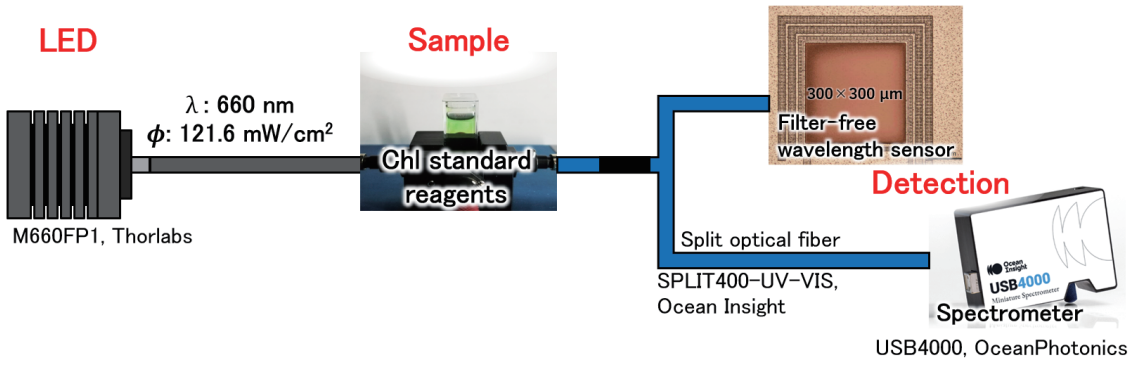

Fig. 6. (Color online) Measurement setup for Chl a/b ratio experiment using Chl standard solution.

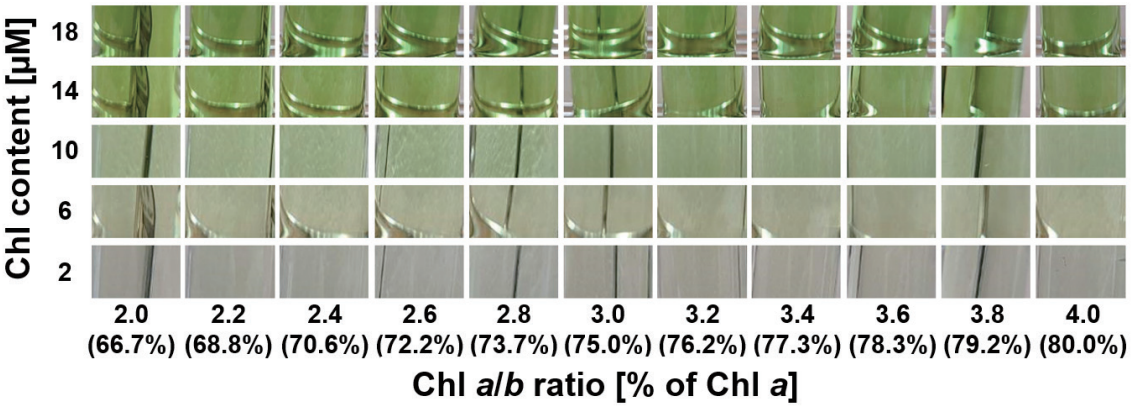

Fig. 7. (Color online) Chl samples used for measurements (Chl content: 2–18 μM, Chl *a*/*b* ratio: 2.0–4.0).

3.2.2 Experimental results

Figure 8 shows the spectra obtained from the spectrometer, demonstrating a decrease in transmitted light intensity with increasing Chl content. For each Chl content, an increase in Chl *a*/*b* ratio was correlated with an increase in the rate of optical absorption near the Chl *a* peak (663 nm) and a decrease near the Chl *b* absorption peak (646 nm). This suggests that absorbance increases with Chl content, and the centroid wavelength shifts toward shorter wavelengths as the Chl *a*/*b* ratio increases.

Figure 9(a) shows a linear relationship between absorbance, measured by the filter-free wavelength sensor, and Chl content, quantified spectroscopically. The more significant absorbance changes observed at 10 and 14 μM are consistent with the spectrometer's quantitative results, likely owing to the lower initial Chl content during sample preparation. Figure 9(b) shows that even with a Chl *a*/*b* ratio range of 2.0–4.0, the absorbance increase varies from approximately 0.51% at a Chl content of 10 μM to 7.58% at a Chl content of 25 μM. This suggests that the filter-free wavelength sensor can accurately measure Chl content across different Chl *a*/*b* ratios, as the absorbance changes are minimal.

Figure 10 shows the measured Chl *a*/*b* ratios. The horizontal axis represents the Chl *a*/*b* ratio quantified using a spectrometer, while the vertical axis shows the sensor current ratio measured

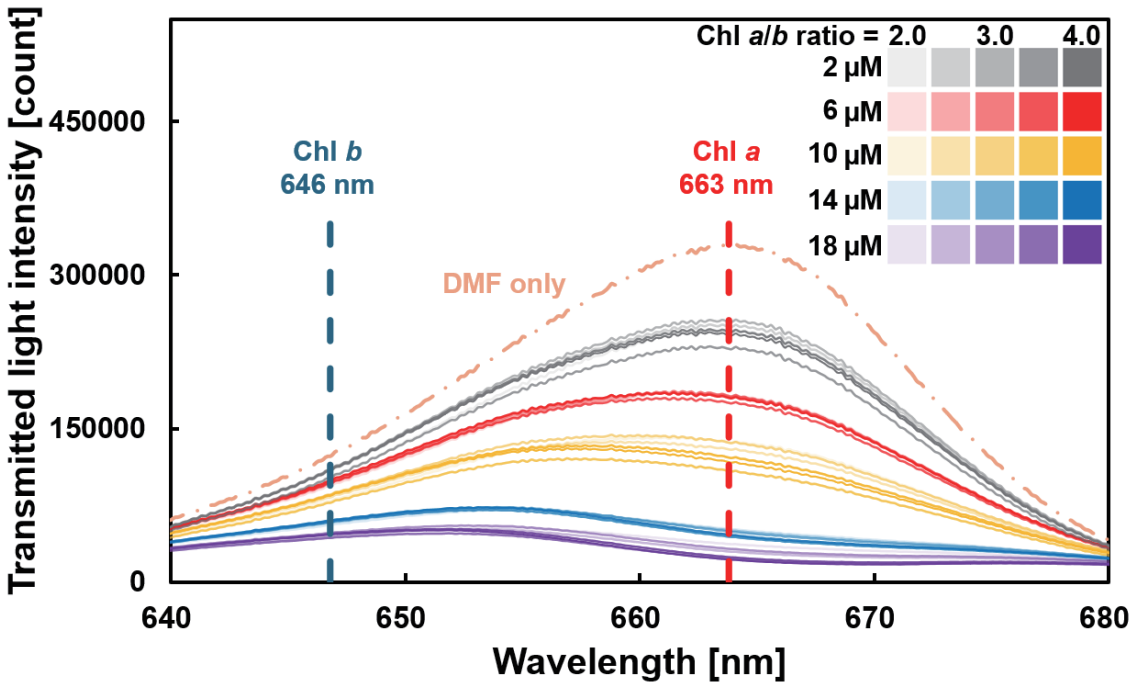

Fig. 8. (Color online) Changes in transmitted light spectral changes at various Chl contents and *a*/*b* ratios. As chlorophyll content increases, the amount of light transmitted through the sample decreases owing to the increase in the rate of light absorption by chlorophyll pigments. The relative proportions of Chl *a* and *b*, as indicated by the Chl *a*/*b* ratio, also affect the spectral shape. A higher Chl *a*/*b* ratio results in increased absorption by Chl *a* and decreased absorption by Chl *b*.

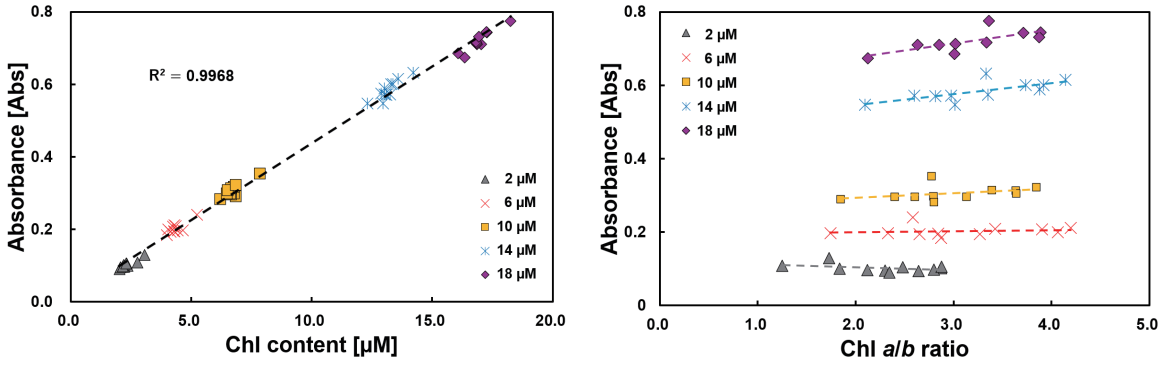

(a) (b)

Fig. 9. (Color online) (a) Relationship between absorbance and Chl content and (b) Chl *a*/*b* ratio. A linear relationship exists between Chl content and absorbance, indicating that changes in Chl *a*/*b* ratio do not significantly impact this relationship.

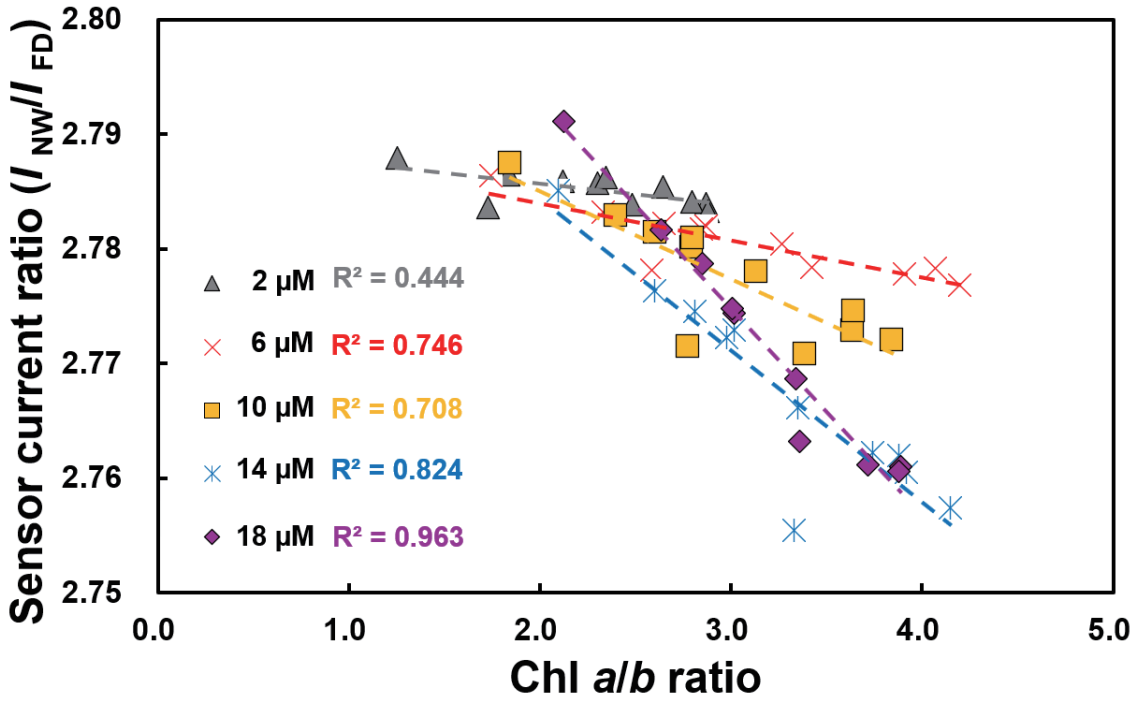

Fig. 10. (Color online) Relationship between sensor current ratio and Chl *a*/*b* ratio. A linear relationship exists between the sensor current ratio and the Chl *a*/*b* ratio. However, the slope and intercept of the linear regression line vary with Chl content.

using the filter-free wavelength sensor. The results indicate a lack of correlation between the sensor current ratio and changes in Chl *a*/*b* ratio. However, a correlation was observed for each specific Chl content. Notably, the measurement variation was more pronounced at lower Chl contents. This is likely due to the relatively low proportion of Chl *b*, constituting only about one-third of the total Chl content. This suggests that the accurate measurement of Chl *b*, particularly

at low concentrations, may be challenging. Indeed, spectrometer quantification revealed that the Chl *b* content at 2 μM ranged from 0.566 to 1.231 μM, confirming its lower abundance.

4. Discussion

Figure 11 shows the relationship between the slope and intercept of the approximate lines in Fig. 10 and absorbance. As shown in the graph, the absorbance of the approximate line increases with Chl content. Consequently, the slope decreases while the intercept increases as the Chl content rises. This trend exhibits a linear relationship, with the coefficients of determination for the slope and intercept being 0.987 and 0.944, respectively. Therefore, it is proposed that the Chl *a*/*b* ratio can be calculated by determining the calibration curve for each Chl content, regardless of variations in Chl content.

Figure 12 shows the changes in Chl a/b ratio for different Chl contents. When the Chl content is 6 μM, an increase in Chl *a*/*b* ratio from 2.0 to 4.0 results in a 0.8 μM increase in Chl *a* content and a 0.8 μM decrease in Chl *b* content. Similarly, when the Chl content is 18 μM, the same change in Chl *a*/*b* ratio leads to a 2.4 μM increase in Chl *a* content and a 2.4 μM decrease in Chl *b* content. This indicates that for the same variation in Chl *a*/*b* ratio, the absolute changes in Chl *a* and *b* contents are higher when the total Chl content is higher. From this result, it can be inferred that a higher Chl content results in a steeper slope. Therefore, instead of calculating the Chl *a*/*b* ratio directly from the sensor current ratio, absorbance measurements should be performed first. Then, using Fig. 11, the necessary calibration curve slope and intercept for Chl *a*/*b* ratio calculation are determined. By using this calibration curve along with the sensor current ratio, variations due to differences in Chl content can be corrected.

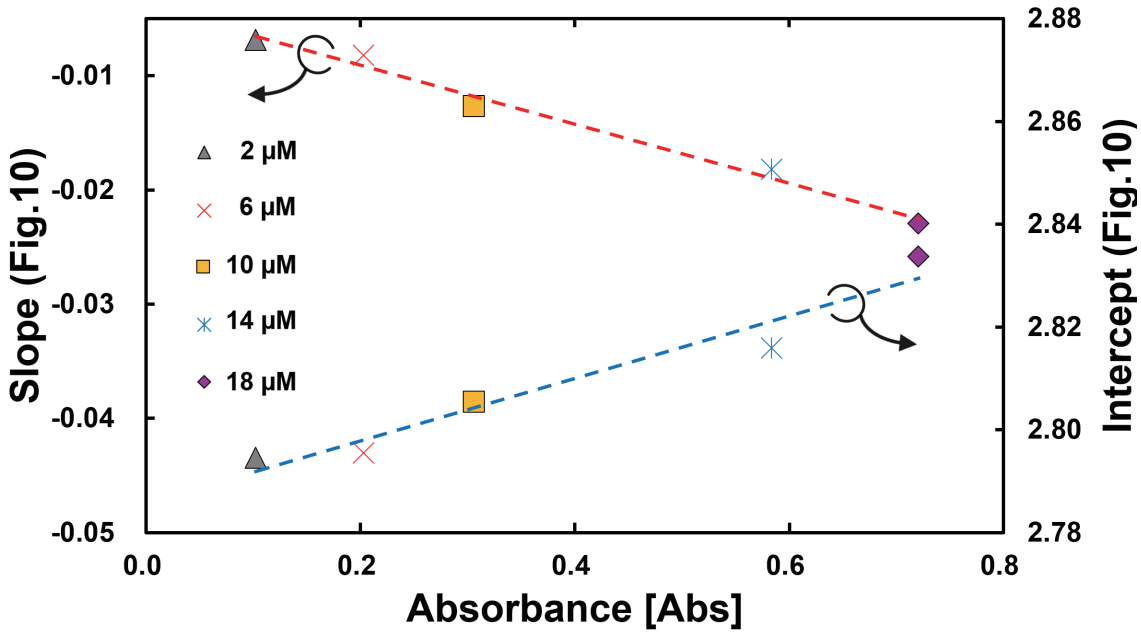

Fig. 11. (Color online) Effect of absorbance (Chl content) on the slope and intercept of the linear fit of Fig. 10.

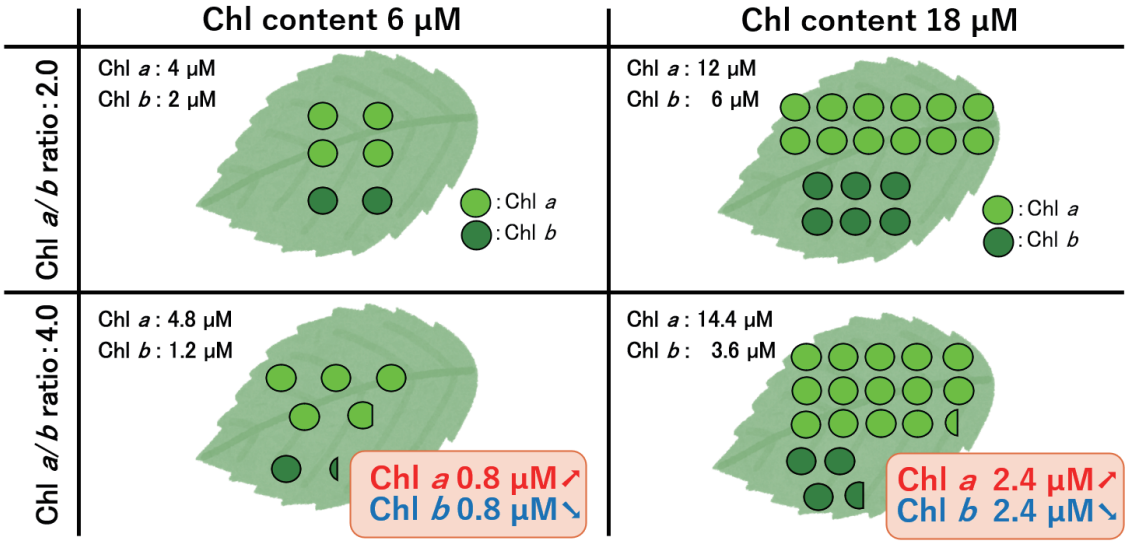

Fig. 12. (Color online) Effect of absorbance (Chl content) on the slope and intercept of the linear fit of Fig. 9.

Figure 13 shows the process for determining the Chl content and Chl *a*/*b* ratio from the I_{NW} and I_{FD} currents measured using the filter-free wavelength sensor. Chl content is calculated by measuring the absorbance derived from the combined I_{NW} and I_{FD} currents. The Chl *a*/*b* ratio is determined through the following steps:

(I) Calibration curve generation: A calibration curve is established by plotting the relationship between the slope and intercept of the calibration curve for the current ratio versus absorbance (Fig. 11)

(II) Calibration curve application: A calibration curve is constructed on a graph of the sensor current ratio against the Chl *a*/*b* ratio (Fig. 10).

(III) Chl *a*/*b* ratio calculation: The Chl *a*/*b* ratio is calculated on the basis of the measured sensor current ratio (I_{NW}/I_{FD}).

By following these steps, the Chl *a*/*b* ratio can be accurately determined.

Figure 14 shows the Chl *a*/*b* ratios determined using the filter-free wavelength sensor and spectrometer. Figure 14(a) shows the Chl *a*/*b* ratio calculated directly from the sensor ratio before quantification. Figure 14(b) shows the Chl *a*/*b* ratio calculated using a calibration curve after quantification. Applying the quantification process significantly improved the coefficient of determination from 0.583 to 0.765, resulting in a 31.2% increase. Additionally, the average error between the spectrometer and sensor measurements decreased from 0.473 to 0.245 after quantification.

The filter-free wavelength sensor used in this study exhibited low noise levels, with dark current values of 25 pA for I_{NW} and 6 pA for I_{FD}. During measurements, the current values were 50 nA for I_{NW} and 18 nA for I_{FD}, resulting in a S/N ratio of approximately 66.8 dB. Therefore, we attribute the variations in results observed before quantification to factors other than the sensor, such as sample variability. The small sample size and potential unevenness in sample concentration due to micro-pipetting may have contributed to the observed variations. Addressing these factors is crucial to improving the accuracy of Chl determination further.

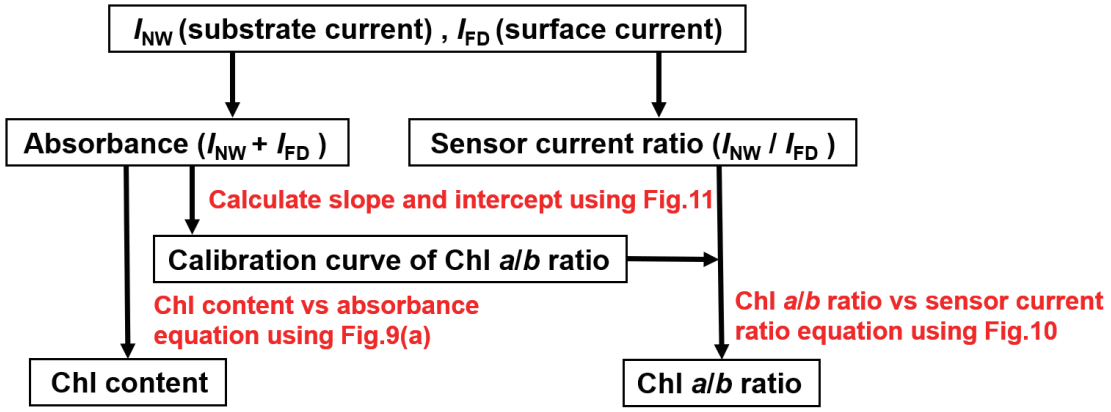

Fig. 13. (Color online) Process for determining Chl content and Chl *a*/*b* ratio using a filter-free wavelength sensor.

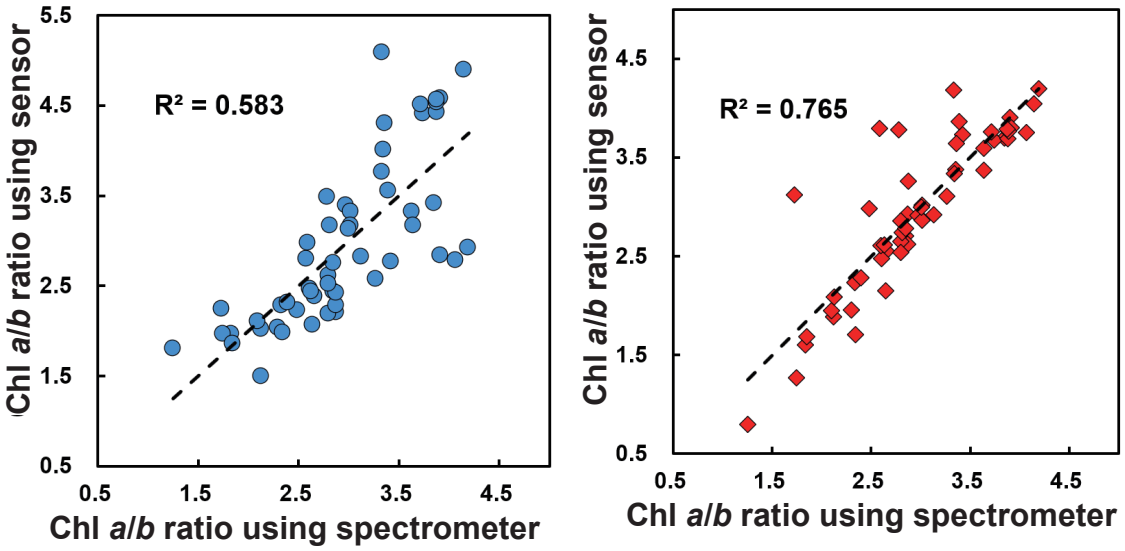

(a) (b)

Fig. 14. (Color online) Comparison of Chl *a*/*b* ratios measured using spectrometer and filter-free wavelength sensor: (a) before and (b) after quantitative analysis.

5. Conclusions

In this study, we demonstrated the factors affecting the measurement of the Chl *a*/*b* ratio using a filter-free wavelength sensor and proposed a method of quantifying the Chl content and Chl *a*/*b* ratio. First, we conducted a reproduction experiment of Chl *a* and *b* using two light sources. The experimental results demonstrated a linear relationship between the sensor current ratio and the light intensity change, with a coefficient of determination of approximately 0.815. This indicates the feasibility of using the sensor to measure the Chl *a*/*b* ratio. Secondly, we prepared and measured samples with Chl contents and Chl *a*/*b* ratios like those found in actual leaves, utilizing standard Chl *a* and *b* solutions. By comparing the Chl *a*/*b* ratios obtained from

the sensor with those from a conventional spectrophotometer, we confirmed that the sensor's absorbance can be used to measure Chl content. However, the measured Chl *a*/*b* ratios exhibited significant variability. Upon further analysis, we concluded that the variation in Chl *a*/*b* ratio was likely due to the decreasing relative abundance of Chl *b* as the total Chl content increased. To address this issue, we developed a calibration curve that relates absorbance (Chl content) to Chl *a*/*b* ratio. This calibration curve improved the coefficient of determination by approximately 31.2% and reduced the variability in Chl *a*/*b* ratio by a factor of 1.93. By utilizing this filter-free wavelength sensor, which is more affordable and compact than conventional measuring instruments, we can accurately determine the Chl *a*/*b* ratio. This advancement has the potential to accelerate agricultural research and enable on-site measurements of the Chl *a*/*b* ratio, ultimately contributing to improved crop productivity.

Acknowledgments

This work was supported by MEXT Initiative to Establish Next-generation Novel Integrated Circuits Centers (X-NICS) under Grant Number JPJ011438 and JSPS KAKENHI Grant Numbers JP23H00182 and JP24K17321.

References

1 United Nations Information Centre: https://www.un.org/en/UN-projects-world-population-to-peak-within-this-century (accessed October 2024).
2 Science Council of Japan: SCJ. **26** (2021) 96 (in Japanese). https://doi.org/10.5363/tits.26.1_96
3 R. Murakami: JEPA **21** (2024) 49 (in Japanese). https://doi.org/10.34471/jeps.21.1_49
4 A. Mizuno: J. Korean Econ Stud. **17** (2020) 51 https://doi.org/10.15017/4738333
5 S. Yasuoka: JRSJ **35** (2017) 362 (in Japanese). https://doi.org/10.7210/jrsj.35.362
6 H. Azadi, S. M. Moghaddam, S. Burkart, H. Mahmoudi, S. Van Passel, A. Kurban, and D. Lopez-Carr: J. Cleaner Prod. **319** (2021) 128602. https://doi.org/10.1016/j.jclepro.2021.128602
7 B. B. Sinha and R. Dhanalakshmi: Future Gener. Comput. Syst. **126** (2021) 169. https://doi.org/10.1016/j.future.2021.08.006
8 A. Rettore de Araujo Zanella, E. da Silva, and L. C. Pessoa Albini: Array **8** (2020) 100048. https://doi.org/10.1016/j.array.2020.100048.
9 H. Imahori and Y. Mori: High Polymes **52** (2003) 331 (in Japanese). https://doi.org/10.1295/kobunshi.52.331
10 R. G. Herrmann and B. A. Larkins: Plant Molecular Biology 2 (Springer. Boston 1991) pp. 449–459. https://doi.org/10.1016/j.bbabio.2010.12.007
11 I. Schumacher, D. Menghini, S. Ovinnikov, M. Hauenstein, N. Fankhauser, C. Zipfel, S. Hörtensteiner, and S. Aubry: Plant J. **109** (2022) 1473. https://doi.org/10.1111/tpj.15645
12 R. Tanaka and A. Tanaka: Biochim. Biophys. Acta, Bioenerg. **1807** (2011) 968. https://doi.org/10.1016/j.bbabio.2011.01.002
13 A. G. Koziol, T. Borza, K.-I. Ishida, P. Keeling, R. W. Lee, and D. G. Durnford: Plant Physiol. **143** (2007) 1802. https://doi.org/10.1104/pp.106.092536
14 A. Tanaka and R. Tanaka: Curr. Opin. Plant Biol. **9** (2006) 248. https://doi.org/10.1016/j.pbi.2006.03.011
15 A. Tanaka, H. Ito, R. Tanaka, N. K. Tanaka, K. Yoshida, and K. Okada: Proc. Natl. Acad. Sci. **95** (1998) 12719. https://doi.org/10.1073/pnas.95.21.12719
16 T. R. B. da Silva, A. C. de S. Reis, and C. D. de G. Maciel: Ind. Crops Prod. **39** (2012) 135. https://doi.org/10.1016/j.indcrop.2012.02.008
17 I. R. Rodriguez and G. L. Miller: HortScience **35** (2000) 751. https://doi.org/10.21273/hortsci.35.4.751
18 Z. Kamarianakis and S. Panagiotakis: Sensors **23** (2023) 2699. https://doi.org/10.3390/s23052699
19 W. J. Moses, A. A. Gitelson, S. Berdnikov, and V. Povazhnyy: Environ. Res. Lett. **4** (2009) 045005. https://doi.org/10.1088/1748-9326/4/4/045005

20 X. Hu, T. Gu, I. Khan, A. Zada, and T. Jia: Cells **10** (2021) 3134. https://doi.org/10.3390/cells10113134.
21 L. A. Brown, O. Williams, and J. Dash: Agric. For. Meteorol. **323** (2022) 109059. https://doi.org/10.1016/j.agrformet.2022.109059
22 F. A. Almomani and B. Örmeci: Environ. Monit. Assess. **190** (2018) 90. https://doi.org/10.1007/s10661-018-6468-y
23 L. Limantara, M. Dettling, R. Indrawati, Indriatmoko, and T. H. P. Brotosudarmo: Procedia Chem. **14** (2015) 225. https://doi.org/10.1016/j.proche.2015.03.032
24 Y.-J. Choi, N. Watanabe, K. Takahashi, S. Toda, K. Takayama, T. Noda, and K. Sawada: Jpn. J. Appl. Phys. **61** (2022) SD1041. https://doi.org/10.35848/1347-4065/ac6387
25 Y.-J. Choi, T. Sakae, K. Nakano, R. Mibu, R. Matsubara, T. Ide, K. Takahashi, T. Noda, H. Ishii, and K. Sawada: ECS Trans. **112** (2023) 139. https://doi.org/10.1149/11201.0139ecst
26 R. Mibu, R. Ichikawa, Y.-J. Choi, T. Ide, S. Toda, K. Takahashi, K. Takayama, T. Noda, and K. Sawada: Proc. 2023 22nd Int. Conf. Solid-State Sensors, Actuators and Microsystems (Transducers, 2023) 729. https://ieeexplore.ieee.org/abstract/document/10516877
27 T. Ide, Y.-J. Choi, R. Matsubara, Y. Kimura, K. Murakami, T. Hizawa, D. Akai, Y. Noda, K. Takahashi, H. Ishii, T. Noda, and K. Sawada: Sens. Actuators, A **360** (2023) 114499. https://doi.org/10.1016/j.sna.2023.114499
28 Y.-J. Choi, T. Sakae, T. Ide, K. Takahashi, T. Noda, and K. Sawada: Appl. Phys. Express. **16** (2023) 012012. https://doi.org/10.35848/1882-0786/acae69
29 T. Ide, Y.-J. Choi, R. Matsubara, I.-H. Kwon, Y. Kimura, K. Murakami, Y. Noda, D. Akai, T. Hizawa, H. Ishii, K. Takahashi, T. Noda, and K. Sawada: Sens. Actuators, A **365** (2024) 114816. https://doi.org/10.1016/j.sna.2023.114816
30 X. Hu, A. Tanaka, and R. Tanaka: Plant Methods **9** (2013) 19. https://doi.org/10.1186/1746-4811-9-19
31 D. I. Arnon: Plant Physiol. **24** (1949) 1. https://doi.org/10.1104/pp.24.1.1
32 R. Esteban, J. I. García-Plazaola, A. Hernández, and B. Fernández-Marín: New Phytol. **217** (2018) 474. https://doi.org/10.1111/nph.14932
33 M. Chazaux, C. Schiphorst, G. Lazzari, and S. Caffarri: Plant J. **109** (2021) 1630. https://doi.org/10.1111/tpj.15643
34 R. J. Porra, W. A. Thompson, and P. E. Kriedemann: Biochim. Biophys. Acta, Bioenerg. **975** (1989) 384. https://doi.org/10.1016/S0005-2728(89)80347-0

About the Authors

Ryoma Mibu received his B.S. degree in electrical and electronic information engineering from Toyohashi University of Technology, Aichi, Japan, in 2023. Currently, he is a graduate student pursuing a master's degree at Toyohashi University of Technology. He is engaged in the research and development of systems using sensors developed by his research group.
(mibu.ryoma.av@tut.jp)

Yong-Joon Choi received his B.S. and M.S. degrees in information technology and electronic education and bio-electronic engineering from Andong National University, Gyeongbuk, Korea, in 2010 and 2013, respectively. He then received his Ph.D. degree in electrical and electronic information engineering from Toyohashi University of Technology (TUT), Aichi, Japan, in 2017. In 2017, he became a postdoctoral researcher at the Department of Electrical and Electronic Information Engineering of TUT, and was subsequently promoted to assistant professor in 2020. Since 2023, he has served as an associate professor in the same department. His research interests focus on the development of CMOS optical biosensors and bio-MEMS.
(choi@ee.tut.ac.jp)

Tomoya Ide received his B.S. and M.S. degrees in electrical and electronic information engineering from Toyohashi University of Technology, Aichi, Japan, in 2020 and 2022, respectively. In 2022, he became a doctoral program student in electrical and electronic engineering at the same university. From 2023 to 2024, he was a research fellow of the Japan Society for the Promotion of Science. From 2024, he was a project research associate at the Institute for Research on Next-Generation Semiconductor and Sensing Science. His current research interests focus on the filter-free CMOS image sensor for bioscience applications. (ide.tomoya.lt@tut.jp)

Yasuyuki Kimura received his B.E. degree from the University of Tsukuba in 1982. He joined SANYO Electric Co., Ltd. in 1982 and had been in charge of developing mixed-signal LSIs. Since 2014, he has been a research fellow at the Department of Electrical and Electronic Information Engineering of Toyohashi University of Technology. (kimura.yasuyuki.db@tut.jp)

Kazuhiro Takahashi received his B.S. degree in mechanical engineering from Nagoya University, Japan, in 2003 and his M.S. and Ph.D. degrees in electrical engineering from the University of Tokyo, Japan, in 2005 and 2008, respectively. From 2008 to 2009, he was a postdoctoral researcher at the Institute of Industrial Science (IIS) of The University of Tokyo. In 2009 and 2018, he respectively became an assistant professor and an associate professor of electrical and electronic information engineering at Toyohashi University of Technology (TUT). In 2022, he became a full professor at the Institute for Research on Next-Generation Semiconductor and Sensing Science (IRES2), TUT. His research interest is in the development of CMOS-MEMS sensors and actuators for optical and biological applications. (takahashi@ee.tut.ac.jp)

Toshihiko Noda received his B.E. and M.E. degrees in electrical and electronic engineering in 2001 and 2003, respectively, and his Ph.D. degree in engineering in 2006 from Toyohashi University of Technology (TUT), Aichi, Japan. He was a postdoctoral researcher and an assistant professor at TUT from 2006 to 2008. Since 2009, he has been an assistant professor at Nara Institute of Science and Technology (NAIST) in Nara, Japan. In 2018, he joined the faculty at TUT and is currently an associate professor at the Institute for Research on Next-Generation Semiconductor and Sensing Science. His current research focuses on multimodal sensing systems and broad sensing technologies based on CMOS array sensors. (noda.toshihiko.zk@tut.jp)

Kotaro Takayama is a professor at the Department of Mechanical Engineering, Toyohashi University of Technology, and the Department of Food Production Science, Ehime University, conducting interdisciplinary research integrating engineering and agriculture. He earned a Ph.D. in agricultural engineering from The University of Tokyo in 2004, became an assistant professor at Ehime University, and was promoted to full professor in 2017. In 2018, he joined Toyohashi University of Technology under a cross-appointment system. His innovations, such as a chlorophyll fluorescence imaging robot and a real-time photosynthesis/transpiration monitoring chamber, are commercially available in Japan. These technologies assess plant photosynthetic activity, growth, and environmental responses in commercial greenhouses and plant factories. He has served as a council member of the Science Council of Japan (2020-) and led projects for Japan's Ministry of Agriculture, Forestry and Fisheries and Ministry of the Environment on AI-driven environmental control and semi-closed greenhouse systems.

Kazuaki Sawada received his B.A. and M.S. degrees in electrical and electronic engineering in 1986 and 1988, respectively, and his Ph.D. degree in system and information engineering in 1991, all from Toyohashi University of Technology (TUT), Aichi, Japan. From 1991 to 1998, he was a research associate in the Research Institute of Electronics, Shizuoka University, Shizuoka, Japan. In 1998, he joined the Department of Electrical and Electronic Engineering, TUT, where he is now serving as a full professor. He is the director of the Institute for Research on Next-Generation Semiconductor and Sensing Science, TUT. He was a guest professor at the Technical University of Munich in 2005. His current research interests focus on the development of nonlabel bio-image sensing devices and multimodal sensors for ion image sensing devices. He is a recipient of the Prizes for Science and Technology, The Commendation for Science and Technology by the Minister of Education, Culture, Sports, Science and Technology of Japan in 2012.
(kazuaki.sawada@tut.jp)